Prediction of infrared light emission from π-conjugated polymers: a diagrammatic exciton basis valence bond theory

S. Dallakyan,[1] M. Chandross,[2] and S. Mazumdar[3]

[1] *Department of Physics, University of Arizona Tucson, AZ 85721*
[2] *Sandia National Laboratories, Albuquerque, NM 87185-1411*
[3] *Department of Physics and The Optical Sciences Center, University of Arizona, Tucson, AZ 85721*

(Dated: February 1, 2008)

There is currently a great need for solid state lasers that emit in the infrared, as this is the operating wavelength regime for applications in telecommunications. Existing π–conjugated polymers all emit in the visible or ultraviolet, and whether or not π–conjugated polymers that emit in the infrared can be designed is an interesting challenge. On the one hand, the excited state ordering in trans-polyacetylene, the π–conjugated polymer with relatively small optical gap, is not conducive to light emission because of electron-electron interaction effects. On the other hand, excited state ordering opposite to that in trans-polyacetylene is usually obtained by chemical modification that increases the effective bond-alternation, which in turn increases the optical gap. We develop a theory of electron correlation effects in a model π-conjugated polymer that is obtained by replacing the hydrogen atoms of trans-polyacetylene with transverse conjugated groups, and show that the effective on-site correlation in this system is smaller than the bare correlation in the unsubstituted system. An optical gap in the infrared as well as excited state ordering conducive to light emission is thereby predicted upon similar structural modifications.

PACS numbers: 42.70.Jk,71.20.Rv,71.35.-y,78.30.Jw

I. INTRODUCTION

π-conjugated polymers have attracted wide attention in the past decade as light emitting organic semiconductors. Light emitting diodes with π-conjugated polymers as emissive materials have reached very high efficiencies and lifetimes[1], and there has also been considerable activity in the area of lasing using organic materials since the original demonstration of spectral narrowing in these systems under intense optical pumping[2,3,4]. One serious limitation in this area has been, however, that all light emitting π-conjugated polymers to date emit in the visible or UV. Telecommunications use infrared radiation, so lasing at these wavelengths is desirable[5]. Whether or not π-conjugated polymers can be synthesized that have light emission in the IR, and what should be the structural features of such a polymer are interesting theoretical questions. Theoretical work on these topics was recently initiated by one of us and his collaborators[6,7], where however, the emphasis was on explaining the unexpectedly high experimentally observed photoluminescence (PL) efficiency in polydiphenylacetylenes (PDPA)[8,9,10], which consist of a backbone carbon chain that is the same as in nonemissive polyenes and side groups that are phenyl groups instead of atomic hydrogen. It was claimed that in an ideal long chain of PDPA the optical gap is smaller than that in trans-polyacetylene (t-PA). Real PDPAs emit in the visible because of their finite conjugation lengths[8], but it was claimed in the earlier theoretical work[6,7] that relatively small optical gaps and strong PL would be expected in any π-conjugated polymer where in addition to longitudinal conjugation there occurs conjugation over a few molecular bonds in the transverse direction.

PDPA's, however, because of their complicated electronic structures cannot be considered as the prototype of these novel class of materials. Furthermore, although the previous calculations[6,7] were carried out to a high level of accuracy using the multiple reference doubles configuration interaction (MRDCI) technique, by themselves they do not give a clear mechanistic explanation of *why* the ordering of the excited energy states in PDPA's are opposite to that in the linear polyenes such that light emission becomes feasible In the present paper we therefore choose the simplest model system that shares the structural feature of transverse conjugation with PDPA's, and analyse its lowest excitations. We demonstrate that finite transverse conjugation over a few bonds is the key to obtaining light emission in the IR (provided, of course, long chain systems can be synthesized). Our theoretical work shows that there exists a different mechanism for the energy crossover between the lowest one- and two-photon states in π-conjugated polymers than the more common one that depends on effective bond alternation[11,12]. The simplicity of our model system allows us to perform numerical work using a diagrammatic exciton basis valence bond method[13] within which the basis functions retain their local character, and diagrammatic interpretations of wavefunctions can be given. A complete insight to the theory of excited state ordering in these complicated systems is thus obtained, which at the same time fully supports the conclusions of our earlier work[6,7] that used a more traditional approach. To the best of our knowledge, although the exciton basis has often been used in the past for calculations on coupled two-level systems (often

though with severe approximations)[14,15,16,17,18,19,20,21], there exist few such calculations for coupled multilevel systems[22,23,24], again sometimes within simpler models. Additional interest of our work then comes from its applicability to realistic multilevel systems.

Emission in the IR would require π-conjugated polymers whose optical gaps are smaller than or comparable to that of t-PA. Linear polyenes and t-PA are, however, weakly emissive, because the lowest two-photon state, the $2A_g$, occurs below the optical $1B_u$ state in these[25]. The same is also true for long-chain polydiacetylenes (PDAs).[26]. This is a conseqence of moderate electron-electron (e-e) interactions between the π-electrons, and is by now well understood[15,25,27,28,29]. The optically pumped $1B_u$ in these systems decays to the $2A_g$ in ultrafast times, and radiative transition from the $2A_g$ to the ground state $1A_g$ is forbidden. Strong PL in systems like poly-paraphenylenevinylene (PPV) and poly-paraphenylene (PPP) implies excited state ordering $E(2A_g) > E(1B_u)$ [where E(...) is the energy of the state], which is a consequence of enhanced bond alternation within the *effective* linear chain model for these systems[11,12]. Within the effective model, the lowest excitations of systems containing phenyl rings as part of the conjugated main chain can be mapped onto those of a linear chain with bond alternation that is much larger than that in t-PA. Explicit calculations then indicate that even with the same e-e interactions, chains with larger bond alternation can have $E(2A_g) > E(1B_u)$. Since enhanced bond alternation necessarily *increases* $E(1B_u)$, it appears that strong PL should then be limited to systems with optical gaps larger than that of t-PA, and emission in the IR from π-conjugated polymers would be impossible.

Our goal is to demonstrate that materials obtained by "site-substitution" of t-PA, in which the hydrogen atoms of t-PA are replaced with transverse conjugated groups will simultaneously have small optical gaps *and* $E(2A_g) > E(1B_u)$. The physical reasoning for this is as follows. Systems obtained by such site-substitution consist of units that are molecular (for example, transstilbene in the case of PDPA), and consecutive units are linked by a single longitudinal bond. With moderate e-e interactions, the ground state can be thought of as covalent (all atomic sites singly occupied). Optical excitation involves intra- and inter-unit one-electron hoppings that generate double occupancies on the units. Since the unit consists of a large molecule in the case of the substituted polyene, this double occupancy occupies the antibonding molecular orbital of the unit, which is delocalized over the entire unit. Thus the *effective* on-site Coulomb interactions (the effective Hubbard interaction, hereafter U_{eff}) is smaller, and this can simultaneously give smaller $E(1B_u)$ (relative to t-PA) and $E(2A_g) > E(1B_u)$. This particular idea is related to a very similar idea in the area of organic conducting charge-transfer solids, where it has long been believed that by going to a larger organic molecule [for example from TMTTF, tetrathiafulvalene to BEDT-TTF, bis(ethylenedithio)fulvalene] the molecular Hubbard U decreases[30]. The only difference in the present case is that we are comparing the bare Hubbard U (in t-PA) and a molecular U_{eff} (in the substituted material), and that the interunit one-electron hopping here is much larger (comparable to the intraunit hoppings) than in the charge-transfer solids, so that molecular exciton ideas have to applied with caution.

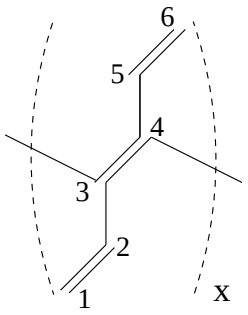

FIG. 1: The model substituted polymer, poly-diethylenepolyacetylene. The numbers are indices for the atomic sites wthin each unit (see text).

We consider here the simplest possible π-conjugated polymer with conjugated sidegroup, the hypothetical system poly-diethylenepolyacetylene, shown in Fig. 1, in which all hydrogen atoms of t-PA have been replaced by ethylene groups. The reason for choosing this hypothetical system is that precisely because of its simple electronic structure, it can be considered as the prototype model for this class of (future) materials. In addition, in order to illustrate the theoretical result we are after we need a physical system for which, (a) accurate many-body computations can be done within a minimal basis (since for any realistic system with large molecular units full configuration interaction, FCI, with the complete basis is out of the question) for relatively long chains, and (b) proper justifications can be given for ignoring basis functions beyond the minimal basis. Note that (b) is at least as important as (a), since it is known that the $2A_g$ can occur above the $1B_u$ also because of incomplete CI[25,31]. Thus for our study to be complete it is essential that we prove that our result is *not* a consequence of our choosing the minimal basis. The symmetry and simplicity of our model system, along with the particular basis we have chosen allow us to achieve this.

In the next section we give the Hamiltonian, parameters and the scope of our calculations. In section III we discuss the complete exciton basis for oligomers of the system shown in Fig. 1, following which we discuss our minimal basis, which in this case consists of the highest occupied molecular orbital (HOMO) and lowest unoccupied molecular orbital (LUMO) of each unit. In section IV we present our numerical calculations for the unsubstituted and substituted polyenes to show that there exists a broad range of Hubbard U over which the $2A_g$ is below the $1B_u$ in the unsubstituted polyene, but above it in

the substituted material of Fig. 1. Wavefunction analysis within the exciton basis valence bond (VB) method[13] also shows that the effective correlations in the substituted polyene are smaller. Following this, in section V we give very detailed heuristic but rigorous arguments which show that this result is not a consequence of incomplete CI. The mechanism of the $2A_g$ – $1B_u$ crossover in polyenes is by now understood; specifically, the correlated $2A_g$ state is dominated by a particular *class* of two electron – two hole (2e–2h) excited configurations, viz., covalent configurations that do not contain any double occupancy. Since the $1B_u$ consists of ionic configurations only, there must exist a U where the $1B_u$ energy is higher. Because of the pictorial natures of the wavefunctions in the diagrammatic exciton basis VB method[13], it is possible to classify precisely all possible one electron – one hole (1e–1h) and 2e–2h exciton diagrams. As we show in section V, based on the symmetry properties of our simple model system this information can then be used to demonstrate that the higher energy MOs of the units play insignificant roles in the $2A_g$ – $1B_u$ crossover and that the minimal basis results are therefore accurate.

II. THE THEORETICAL MODEL

We will consider our model polymer system within the simple dimerized Hubbard Hamiltonian,

$$H = H_{1e} + H_{ee} \tag{1a}$$

$$H_{1e} = -\sum_{\langle ij\rangle,\sigma} t_{ij} c^{\dagger}_{i,\sigma} c_{j,\sigma} \tag{1b}$$

$$H_{ee} = U \sum_{i} n_{i,\uparrow} n_{i,\downarrow} \tag{1c}$$

In the above, H_{1e} describes one-electron nearest neighbor hoppings of electrons, and H_{ee} consists of the electron-electron (e-e) interaction within the Hubbard approximation. The Fermion operator $c^{\dagger}_{i,\sigma}$ creates a π-electron of spin σ on site i, $n_{i,\sigma}$ is the number of electrons with spin σ on site i, and $\langle..\rangle$ implies nearest neighbors. The one-electron hopping integrals t_{ij} are taken to be $t_1 = 2.4(1 - \delta)$ eV, and $t_2 = 2.4(1 + \delta)$ eV, with $\delta = 0.07$, corresponding to single and double bonds, respectively. These values of the hopping integrals are considered standard for π-conjugated systems. We have ignored all Coulomb interactions other than the on-site repulsion U, since the $2A_g$ - $1B_u$ crossover is related to this interaction only, with the spin-independent long range intersite Coulomb interactions merely modifying the magnitude of U at which the crossover occurs. Nonzero intersite Coulomb interactions make our exciton basis calculations much more complicated, without providing fundamentally new insight.

Within the Hamiltonian of Eq. (1), the $2A_g$ occurs above the $1B_u$ at $U = 0$ in linear polyenes. For nonzero δ, as U is increased from zero, there exists a *finite* U_c at which the $2A_g$ - $1B_u$ crossover occurs, and the $2A_g$ now occurs below the $1B_u$[11,12,28]. We perform similar calculations for oligomers of the the substituted materials, polydiethylenepolyacetylene (Fig. 1) here. For our hypotheses in section I to be correct the following should be true. First, not only should the optical gap in the substituted polyene be smaller than that of the corresponding polyene with the same number of backbone chain carbon atoms at all U, but the rate of increase of $E(1B_u)$ with U must also be smaller. The latter ia a definite signature of smaller effective correlation U_{eff}. Second, if U_{eff} is indeed smaller than the bare U in the substituted polyene, the bare U_c at which the $2A_g$ - $1B_u$ crossover occurs in the substituted polyene must be larger than in the unsubstituted polyene. As a consequence, for a given e-e interaction it becomes possible to have the $2A_g$ above the $1B_u$ in the substituted polyene even as it is below the $1B_u$ in the unsubstituted polyene.

III. DIAGRAMMATIC EXCITON BASIS FOR POLYDIETHYLENE-ACETYLENE

A. The complete basis

It is clear that accurate many-body calculations for oligomers with the structure of Fig. 1 as the repeat unit can only be done within a reduced basis. The reduced basis cannot be within the configuration space, as it would be simply incorrect to ignore atomic orbitals. A common approach in such cases is often to perform CI calculations using a limited basis of molecular orbitals (MOs), but this is not suitable in the present case: MOs are delocalized over the entire space, and within the MO approach there is simply no information on the connectivity between the atoms that can allow choosing the reduced basis. It is for this reason that we have chosen the exciton basis VB method, which was previously used to perform exact calculations within the Pariser-Parr-Pople model[32,33] for linear polyenes and to obtain diagrammatic wavefunctions[13]. As noted there, the exciton basis VB method is a hybrid of configuration space VB and the momentum-space MO pictures, and thus the basis functions within this approach retain the full information on the connectivity between the atoms (as in configuration space) while at the same time, as in MO theory, the basis functions can be given certain hierarchy from energetic considerations. As we show later, both of these are essential for choosing the minimal basis as well as its justification.

As in the case of polyenes[13] we arrive at the exciton basis by rewriting the one-electron term H_{1e} in Eq. 1(b) as a sum of two terms, one intra-unit and the other inter-unit,

$$H_{1e} = H_{1e}^{intra} + H_{1e}^{inter} \tag{2}$$

The intra-unit part of the Hamiltonian is the simple

Hückel Hamiltonian for the hexatriene units,

$$H_{1e}^{intra} = -\sum_{\mu}\sum_{j=1}^{5} t_{j,j+1}[c^{\dagger}_{\mu,j,\sigma}c_{\mu,j+1,\sigma} + h.c.] \quad (3)$$

where μ is an index for the units and j is an atom within the unit. The inter-unit part of H_{1e} can be similarly written as,

$$H_{1e}^{inter} = -t_1\sum_{\mu}[c^{\dagger}_{\mu,4,\sigma}c_{\mu+1,3,\sigma} + h.c.] \quad (4)$$

where we recognize that the bonds between the units involve the weaker hopping integral t_1 only, and only the atom 4 of the unit of the left unit and the atom 3 of the right unit are bonded (see Fig. 1 for the numbering of the atoms within each unit).

The solutions to H_{1e}^{intra} are the intra-unit local Hückel MOs, described by,

$$\psi^{\dagger}_{\mu,k,\sigma} = \sum_{j=1}^{6} A_{kj}c^{\dagger}_{\mu,j,\sigma} \quad (5)$$

where $k = 1$ – 6, with $k = 3$ and 4 corresponding to the HOMO and LUMO, respectively. The reverse transformation,

$$c^{\dagger}_{\mu,j,\sigma} = \sum_{k=1}^{6} A_{jk}\psi^{\dagger}_{\mu,k,\sigma} \quad (6)$$

where $[A_{jk}] = [A_{kj}]^{-1}$ gives the site-operators in terms of the local MO operators, and can be used to obtain H_{1e}^{inter} in terms of these,

$$H_{1e}^{inter} = -t_1\sum_{\mu}\sum_{k,k',\sigma}[A_{4k}A_{3k'}\psi^{\dagger}_{\mu,k,\sigma}\psi_{\mu+1,k',\sigma} + h.c.] \quad (7)$$

H_{1e}^{inter} when operating on any exciton basis VB diagram leads to interunit charge-transfer (CT), which may involve pairs of bonding MOs, antibonding MOs, or bonding and antibonding MOs. The magnitude, and more importantly the sign, of the CT matrix element depend on the A_{jk}. In the case of linear polyenes, CT involving the bonding MO of the unit on the left lead to positive matrix elements of H_{1e}^{inter}, whereas CT involving the antibonding MO of the left unit lead to negative matrix elements[13]. The same is true here if k, k' in Eq. (7) are limited to the HOMO and LUMO ($k, k' = 3, 4$).

Eq. (6) also enables us to rewrite the Hubbard interaction as,

$$\begin{aligned} H_{ee} &= U\sum_{\mu}\sum_{j=1}^{6}[\sum_{k_1,k_2} A_{jk_1}A_{jk_2}\psi^{\dagger}_{\mu,k_1,\uparrow}\psi_{\mu,k_2,\uparrow}\sum_{k_3,k_4} A_{jk_3}A_{jk_4}\psi^{\dagger}_{\mu,k_3,\downarrow}\psi_{\mu,k_4,\downarrow}] \\ &= U\sum_{\mu}\sum_{j}[\sum_{k_1,k_2}|A_{j,k_1}|^2|A_{j,k_2}|^2N_{\mu,k_1,\uparrow}N_{\mu,k_2,\downarrow} + \sum_{k,k_1,k_2}|A_{j,k}|^2\cdot A_{j,k_1}A_{j,k_2}N_{\mu,k,\uparrow}\psi^{\dagger}_{\mu,k_1,\downarrow}\psi_{\mu,k_2,\downarrow} + \\ &+ \sum_{k,k_1,k_2}|A_{j,k}|^2\cdot A_{j,k_1}A_{j,k_2}N_{\mu,k,\downarrow}\psi^{\dagger}_{\mu,k_1,\uparrow}\psi_{\mu,k_2,\uparrow} + \sum_{k_1\neq k_2}\sum_{k_3\neq k_4} A_{j,k_1}A_{j,k_2}A_{j,k_3}A_{j,k_4}\psi^{\dagger}_{\mu,k_1,\uparrow}\psi_{\mu,k_2,\uparrow}\psi^{\dagger}_{\mu,k_3,\downarrow}\psi_{\mu,k_4,\downarrow}] \end{aligned} \quad (8)$$

Here $N_{\mu,k,\sigma} = \psi^{\dagger}_{\mu,k,\sigma}\psi_{\mu,k,\sigma}$, the number of electrons with spin σ in the kth MO of the μth unit. Thus H_{ee} contains diagonal density-density terms, as well as off-diagonal density-electron transfer and electron transfer-electron transfer terms within the exciton basis. All terms, however, are local (i.e., intraunit), and electron-transfers due to the Hubbard interaction are strictly between the MOs of the same unit. If the units possess both center of inversion and charge-conjugation symmetry (as is true here), an additional simplification occurs when calculations are carried out within a reduced basis containing pairs of MOs related by charge-conjugation symmetry[13], viz., terms containing products of density and electron transfer vanish exactly[13]. This is because the product $A_{j,k_1}A_{j,k_2}$ in the density - electron transfer term has different signs for sites j that are related by spatial symmetry. Of course when considering the effects of the MOs not included in the reduced basis the effects of these terms have to be considered.

B. The minimal basis

The complete Hamiltonian, $H_{1e} + H_{ee}$ is way beyond our reach for any system containing more that two units of the substituted polyene of Fig. 1. At the same time, we show in section V that the two-unit oligomer is a special case, and is not of interest. We therefore work within a minimal basis which is chosen as follows. We first solve H_{1e}^{intra} and note the following: (i) the HOMO-LUMO gap is much smaller than the other bonding to antibonding energy gaps (see Fig. 2 for the single-particle energies), and (ii) H_{1e}^{inter} involves only atoms 3 and 4 of each unit, and the contributions by the HOMO – 1

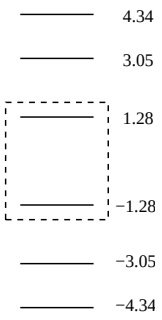

FIG. 2: The single-particle energies (in eV) for each isolated unit, with standard hopping integrals (see text). The dashed box indicates our minimal basis.

and LUMO + 1 levels to the electron densities on these atoms ($A_{j,k}$ in Eq. (6) for k = 2 and 5) are relatively small [$|A_{j,1}| = |A_{j,6}| = 0.52$, $|A_{j,2}| = |A_{j,5}| = 0.21$, $|A_{j,3}| = |A_{j,4}| = 0.43$, where $j = 3$ and 4], although the contributions by the outermost single-particle levels $k = 1$ and 6 are large again (note, however, that the single-particle energy gaps between these last pair of MOs is rather large, from Fig. 2). We therefore construct our minimal basis using only the HOMO and the LUMO and retain only $k, k' = 3$ and 4 in Eqs. 7 and 8. Since these MOs are related by charge-conjugation symmetry the density - electron transfer terms (but not the electron transfer – electron transfer term) in H_{ee} vanish exactly within our minimal basis and the minimal exciton basis Hamiltonian is very similar to the one considered before for polyenes[13], except that the A_{jk} are very different now ($|A_{jk}| = 2^{-1/2}$ in polyenes). Note in particular that with H_{ee} limited to the Hubbard interaction the remaining electron transfer – electron transfer term in H_{ee} consists of two electron transfers involving opposite spins only, and therefore virtual excitations involving the outer MOs do not occur. The lower occupied MOs therefore contribute a constant to the diagonal matrix elements of the exciton basis VB diagrams, which is the frozen core approximation.

While single-particle energies and electron densities give guidance to the choice of the minimal basis, *justification* of the minimal basis requires the demonstration that the minimal basis can satisfactorily reproduce the results expected for the complete Hilbert space. This is easily done for the one-electron part of the Hubbard Hamiltonian, H_{1e}. We solve the full Hückel Hamiltonian for oligomers with number of backbone carbon atoms N = 4 – 10, and compare the exact lowest excitation energies with the approximate excitation energies obtained using the minimal exciton basis. Excellent agreement is found, as is shown in Table 1, where we compare the energies of 1e–1h B_u excitations for N = 4 – 10 (the 1e–1h A_g excitation energies can be obtained from the B_u energies and are therefore not given separately).

Justification of the minimal basis even when H_{ee} is nonzero is much more complicated. We postpone this until after we present our numerical demonstration within the minimal basis that the $1B_u$ optical gap is smaller in the substituted polyene even when U is included, and the U_c at which the $2A_g$ becomes lower than the $1B_u$ is much larger for the substituted system. As mentioned in section I, we are able to give a very complete proof that our reasult of higher U_c is not a consequence of incomplete CI, based on symmetry properties of exciton basis VB diagrams.

C. The mechanism of the $2A_g - 1B_u$ crossover

Although in reference 13 detailed discussions of exciton basis VB diagrams for the case of linear polyenes were presented, in view of what follows in this and the next sections, it is useful to reemphasize some of these. We therefore discuss the mechanism of the $2A_g$ – $1B_u$ crossover within the the exciton basis VB approach. While it is known that the occurrence of the $2A_g$ below the $1B_u$ is a correlation effect that introduces strong configuration mixing between the "ground state" configuration and 2e–2h configurations, a key theme here is that only a specific *class* of 2e–2h states is actually relevant.

Polyene exciton basis VB diagrams, and the substituted polyene exciton basis VB diagrams within the minimal basis are coupled by H_{1e}^{inter} and H_{ee}. We give here the complete expressions for $c_{\mu,3,\sigma}$ and $c_{\mu,4,\sigma}$ such that the effects of H_{1e}^{inter} (see Eq. (7)) can be understood.

$$c_{\mu,3,\sigma} = -0.52\psi_{\mu,1,\sigma} + 0.21\psi_{\mu,2,\sigma} + 0.43\psi_{\mu,3,\sigma} + 0.43\psi_{\mu,4,\sigma} - 0.21\psi_{\mu,5,\sigma} - 0.52\psi_{\mu,6,\sigma} \quad (9a)$$

$$c_{\mu,4,\sigma} = -0.52\psi_{\mu,1,\sigma} - 0.21\psi_{\mu,2,\sigma} + 0.43\psi_{\mu,3,\sigma} - 0.43\psi_{\mu,4,\sigma} - 0.21\psi_{\mu,5,\sigma} + 0.52\psi_{\mu,6,\sigma} \quad (9b)$$

All numerical coefficients in the above are obtained from the invert of the Hückel wavefunction matrix for linear hexatriene. The relative signs (though not magnitudes) between the coefficients of the bonding and antibonding MOs in the site operators for the polyenes are the same as those between the coefficients of the HOMO and LUMO ($\psi_{\mu,3,\sigma}$ and $\psi_{\mu,4,\sigma}$) for the substituted polyene in the above. Thus in the following both systems can be described simultaneously. Note that H_{1e}^{inter} from Eqs. (7) and (9) consists of terms $\psi^{\dagger}_{\mu,k,\sigma}\psi_{\mu+1,k',\sigma}$, which can be both positive or negative. These signs will be important in what follows in this section and in section V.

In Fig. 3 we show the VB exciton diagrams and CI channels that are most relevant for the $2A_g$ – $1B_u$ crossover in a two-unit system, which can be either the two-unit polyene or the two-unit substituted polyene with the lower levels completely filled. Each arrow in this and similar figures below corresponds to one application of H_{1e}^{inter} (Eq. (7)) on the VB diagrams to the

States	N = 4		N = 6		N = 8		N = 10	
	Exact Hückel	Exciton VB	Exact Hückel	Exciton VB	Exact Hückel	Exciton VB	Exact Hückel	Exciton VB
$1B_u$	1.81	1.86	1.41	1.54	1.17	1.36	1.02	1.25
$2B_u$	3.37	3.53	2.48	2.69	2.22	2.35	1.99	2.06
$3B_u$			2.89	2.83	2.49	2.37	2.16	2.08
$4B_u$			3.55	3.72	3.05	3.18	2.33	2.66
$5B_u$					3.27	3.22	2.81	2.84
$6B_u$					3.62	3.34	2.97	2.91

TABLE I: Exact versus minimal exciton basis energies (in eV) of the lowest 1e-1h B_u states in oligomers of the substituted polyene at U = 0.

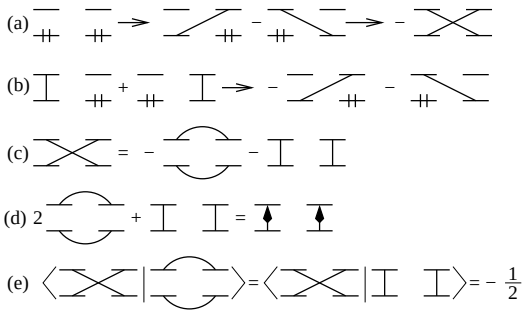

FIG. 3: CI channels and exciton basis VB diagrams relevant for the $2A_g$ – $1B_u$ crossover in a two-unit system with two MOs per unit. Bonding and antibonding MOs of each unit are occupied by 0, 1 and 2 electrons, with pairs of singly occupied sites coupled by singlet bonds (see text). Each arrow in (a) and (b) represents one application of H_{1e}^{inter} on the diagrams on the left, to obtain the diagrams on the right of the arrow. The plus and minus signs of the matrix elements are obtained from Eq. (9), and their magnitudes are not shown. The linear relationship (c) shows that the diagram with crossed bonds is a superposition of two other diagrams with the same orbital occupancies but with noncrossing bonds. The diagram on the right in (d) is triplet–triplet (TT), with two triplets localized on the two units. (e) shows the overlap between the nonorthogonal 2e–2h VB diagrams.

immediate left, to get the VB diagramis to the immediate right of the arrow. As mentioned above, the plus and minus signs here are obtained fron the equations for the site-operators above. Aside from the signs the CI channels should also include the magnitudes $A_{4k}A_{3k'}$, which can again be obtained from Eq. (9), but which are not very important for our discussions.

The first diagram in CI channel (a) is the product wavefunction of the ground states of two noninteracting units, with all electrons in the bonding MOs, which we refer to hereafter as the Simpson ground state[14]. This diagram is symmetric with respect to the mirror plane between the two units, occurs only in the A_g subspace, and dominates the $1A_g$ wavefunction for small to moderate U. One application of H_{1e}^{inter} generates the "minus" linear combination of two charge-transfer (CT) diagrams (two because CT can occur in either direction). The relative minus sign is obtained from Eq. (9). Here and in the following a singlet bond, drawn as a line connecting MOs k and k', on the same or different units, is defined as $2^{-1/2}(\psi^\dagger_{\mu,k,\uparrow}\psi^\dagger_{\mu',k',\downarrow} - \psi^\dagger_{\mu,k,\downarrow}\psi^\dagger_{\mu',k',\uparrow})|0\rangle$ as before[13]. A second application of H_{1e}^{inter}, such that CT is now in the *opposite* direction, generates the 2e–2h charge-neutral diagram with crossed bonds (the last diagram in (a)) which can again occur in the A_g space only. The "minus" sign in front of this diagram in the CI channel shown occurs in the case of both unsubstituted and substituted polyenes, and will be relevant for later discussions.

Fig. 3(b) shows CI channels originating from the superposition of two Frenkel exciton diagrams with intra-unit excitations. The two Frenkel exciton diagrams are absent in the A_g subspace, and the "plus" linear combination shown occurs in the B_u susbspace. Operating with H_{1e}^{inter} on the two Frenkel exciton diagrams generates the same CT diagrams that are generated in the second step in (a), but now with a relative plus sign between them. Because of this relative plus sign a second application of H_{1e}^{inter} (again promoting CT in the opposite direction from the first step) leads to an exact cancellation, such that the diagram with crossed bonds does not occur in the B_u subspace.

The mechanism of the $2A_g$ – $1B_u$ crossover is then as follows. The CT diagrams in Fig. 3 have unequal numbers of electrons on the units, and are hence necessarily ionic in the language of configuration space VB theory. The Frenkel exciton diagrams are also ionic, as can be confirmed by direct expansion of exciton basis operators[13]. The diagram with the crossed bonds in Fig. 3(a), however, is charge-neutral as far as the units are concerned, and as shown in Fig. 3(c) is a superposition of two VB diagrams with noncrossing bonds, which can also be confirmed by expansion of exciton basis operators. Equally importantly, a 2:1 superposition of these last two diagrams (see Fig. 3(d)) corresponds to two triplets, or triplet-triplet (TT) excitation on the two units[13], which is covalent in the language of configuration space VB theory. As has been emphasized by previous authors, the $2A_g$ – $1B_u$ crossover can then be understood

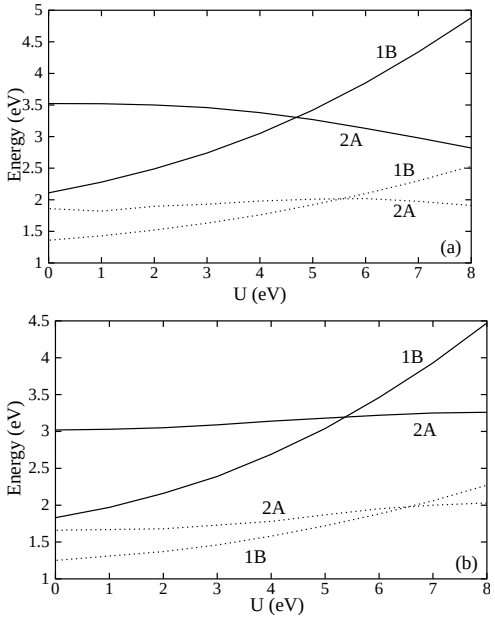

FIG. 4: The excitation energies $E(1B_u)$ and $E(2A_g)$ for the unsubstituted (solid lines) and the substituted polyene (dotted lines), (a) N = 8, (b) N = 10.

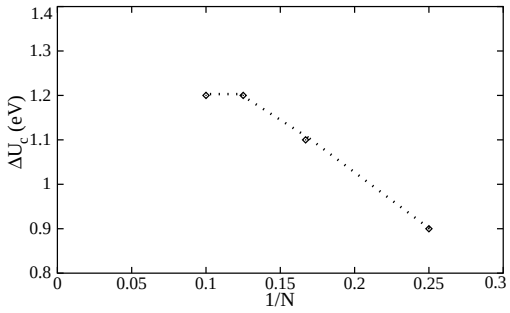

FIG. 5: The difference in U_c between substituted and unsubstituted polyene as a function of $1/N$.

as a competition between CT and TT diagrams. Even though the diagram with crossed bonds is obtained in second order in H_{1e}^{inter} from the Simpson ground state, this second order process can be more important than the first order process leading to the CT diagrams, because of relationship (d), since covalent diagrams have smaller diagonal matrix element of H_{ee} than ionic diagrams. The $2A_g$ is dominated by ionic diagrams at small U and occurs above the $1B_u$, while it is dominated by covalent TT diagrams at moderate to large U and occurs below the $1B_u$. We have discussed the crossover for a two-unit system only. The only new feature in long chains is the occurrence of CT and TT diagrams with long bonds between units that are not neighbors (see reference 13 and below).

IV. NUMERICAL RESULTS WITHIN THE MINIMAL BASIS

We performed exact numerical calculations for N = 4, 6, 8 polyenes and quadruple-CI (QCI) calculations for the N = 10 polyene to determine U_c. Within the exciton basis the Hamiltonian matrix is nonsparse and this is the reason for doing QCI instead of exact calculations for N = 10. As has been shown before[34,35], QCI is excellent for determining the energies of the lowest excitations, the $1B_u$ and the $2A_g$, to high accuracy, at these N. Identical calculations were done within the minimal basis for oligomers of polydiethylene-acetylene. In Fig. 4(a) and (b) we have plotted the excitation energies $E(1B_u)$ and $E(2A_g)$, with respect to the ground state energy ($E(1A_g) = 0$) for N = 8 and 10, respectively. As claimed in section I, $E(1B_u)$ is lower for the substituted polyene in both N = 8 and 10, for all values of U. Note in particular that $E(1B_u)$ for the substituted polyene increases with the bare U much less rapidly than for the unsubstituted polyene, which is a distinct signature that U_{eff} in the substituted material is smaller. The U_c at which $E(2A_g)$ becomes smaller than $E(1B_u)$ in the unsubstituted polyenes is very slightly larger in N = 10 than in N = 8, in agreement with previous work[28]. Importantly, the $2A_g$ remains above the $1B_u$ in the substituted polyene for a much larger range of the Hubbard U, and U_c for the substituted polyene is larger than that of the unsubstituted polyene by about 1 eV. The initial increase in $E(2A_g)$ with U for substituted polyenes in Fig. 4 is real and has been seen previously in density matrix renormalization group (DMRG) studies of long polyene chains by Shuai et. al.[28] (see, in particular, Fig. 1 in this reference). As discussed there, this initial increase is related to the magnitude of the $2A_g$ – $1B_u$ gap at $U = 0$. The smaller this energy gap, the more the tendency to initial increase in $E(2A_g)$ (although $E(2A_g)$ does begin to decrease again at large U). The substituted polyenes considered here have relatively small $2A_g$ – $1B_u$ gap already at N = 10, which explains the behavior of $E(2A_g)$ in Fig. 4. Taken together, the initial increase of $E(2A_g)$, and the less rapid rise in $E(1B_u)$ give the larger U_c in the substituted polyenes. In Fig. 5 we have plotted the difference ΔU_c between the U_c values for the substituted and the unsubstituted polyenes against the chain length N. ΔU_c increases modestly between N = 4 and N = 8, but then is seen to have a tendency to saturation. This behavior of ΔU_c is to be expected from what we have said in the above. The initial increase in ΔU_c is due largely to the initial increase in $E(2A_g)$ with U in the substituted polyene, which occurs for a larger range of U the longer the system is. This in turn is simply a consequence of smaller one-electron $2A_g$ – $1B_u$ gap as N increases. As the chain gets longer, the rate of decrease of the one-electron $2A_g$ – $1B_u$ gap itself decreases and the range of U over which $E(2A_g)$ has initial increase in the substi-

tuted polyene tends to saturate, leading to a tendency of saturation in the U_c as well as ΔU_c. Within the minimal basis therefore, ΔU_c is at least as large as that at N = 10 in the long chain limit. The larger U_c in the substituted polyenes is a direct consequence of the delocalized HOMO and LUMO in the monomer, an effect which is included in the A_{jk}.

Information on the effective Coulomb correlation can also be found from wavefunction analysis. In our previous work we had studied linear polyenes within the Pariser-Parr-Pople model[32,33], for both small bond-alternation (δ = 0.07, where the $2A_g$ is below the $1B_u$, and large bond-alternation ($\delta = 0.3$), for which the $2A_g$ is above the $1B_u$. We had found that while the difference in the $1B_u$ wavefunctions in the two cases was very small, the difference between the $2A_g$ wavefunctions was substantial: the $2A_g$ for small δ is dominated by TT exciton basis diagrams, while for large δ there occurs a strong admixing of 1e–1h CT diagrams. It is then expected that similar differences in the $2A_g$ wavefunctions would occur here for the unsubstituted and substituted polyenes. In Fig. 6 we show the $1B_u$ wavefunctions for the N = 10 polyene and the corresponding substituted polyene for $U = 6$ eV, which is larger than the U_c for the polyene but smaller than the U_c for the substituted polyene. These wavefunctions appear to be very similar in nature. In contrast, the $2A_g$ wavefunctions for the two systems for the same U, are remarkably different, as seen in Fig. 7. While the polyene $2A_g$ is predominantly TT and TT $\otimes$ CT (diagrams which appear to be similar to the TT but in which the lengths of the two interunit bonds are unequal are referred to as TT $\otimes$ CT[13]) there is much stronger admixing of CT diagrams in the case of the substituted polyene, indicating clearly that the effective e-e correlation in the latter is smaller for the same bare U. CT diagrams are necessarily ionic in the language of configuration space VB theory[13,18], and the greater ionicity of the $2A_g$ wavefunction in the substituted polyene is related to its initial rise in energy with U[28].

V. BEYOND THE MINIMAL BASIS, THE ROLE OF HIGHER EXCITATIONS.

A large body of previous work has established that in the case of linear polyenes low order CI using a MO basis does not capture important correlation effects[25,31]. Thus within the the PPP Hamiltonian, double-CI fails to find the $2A_g$ below the $1B_u$ for polyenes with N > 8, and either QCI or MRD-CI becomes necessary to obtain the correct excited state ordering. Similarly, full-CI calculations within the Hubbard model for N = 12 using the six innermost bonding and antibonding MOs also fails to find the correct excited state ordering.[31] Thus the very fact that the minimal exciton basis gives a $2A_g$ – $1B_u$ crossover at all is already significant. Nevertheless, since for each N in polydiethylene-acetylene we ignore more MOs than we retain, it might appear that the numerical result that U_c for this system is much larger than that of polyenes is a simple consequence of our approximation. We show in this section that this is not so, and the higher exciton basis VB diagrams play an insignificant role in the $2A_g$ – $1B_u$ crossover, especially in long chains. There is a fundamental difference between the CI involving completely delocalized MOs and the CI involving the exciton basis VB diagrams. The latter possess local character and are more suitable for calculations involving local Coulomb interactions. We emphasize that even though our discussions below are heuristic and based on physical arguments rather than numerical calculations, they are complete and rigorous.

Our demonstration of the weak role of the higher exciton basis VB diagrams will be done in several steps. First, we look at simple polyenes more closely, to determine that only a certain class of higher excitations can lower $E(2A_g)$ with respect to the $1B_u$. Based on this we arrive at two specific criteria for relevance of higher excitations in polydiethylene-acetylene, viz., that they should also involve crossed bonds (in other words, that the relevant configurations are those that are related to the high energy TT diagrams); and that they are coupled to the lower energy TT diagrams. This allows us to severely limit our search of relevant high energy configurations. We then go through the *complete list* of such configurations, both intra- and interunit, asymmetric and symmetric with respect to the mirror-plane symmetry. Because the two-unit oligomer is a special case (see below) we discuss this separately. Following this we discuss longer oligomers. Our basic conclusion is that the longer the oligomer, the more irrelevant are the high energy configurations. The discussion that follows is unavoidably complex, and we have therefore given a separate summary at the end of this section. The reader uninterested in the details of CI theory and the exciton VB basis can directly go to this summary.

Before we present our discussion of higher MOs in polydiethylene-acetylene, we present additional discussions on the $2A_g$ – $1B_u$ crossover in polyenes that go beyond Fig. 3. Double-CI is not suitable for correct evaluation of $E(2A_g)$ since quadruple excitations that are coupled to the doubly excited configurations, and that can therefore lower $E(2A_g)$, are excluded in double-CI. The CI channel describing this is shown in Fig. 8(a), where the quadruply excited diagram for the two-unit case is obtained from two applications of H_{1e}^{inter} on the VB diagram with crossed bonds in Fig. 3, once again such that the two CT processes are in the opposite direction. $E(2A_g)$ is also lowered by going to larger N. As shown in Fig. 8(b) this is due to CI between the two diagrams with short nearest neighbor and long next-nearest neighbor crossed bonds, again through two applications of H_{1e}^{inter} in opposite directions. Very similar CI process occurs between the final diagram in Fig. 8(b) and the diagram with even longer crossed bonds and so on. Two things will be relevant in our discussions below. First, even though diagrams with long crossed bonds are not directly coupled

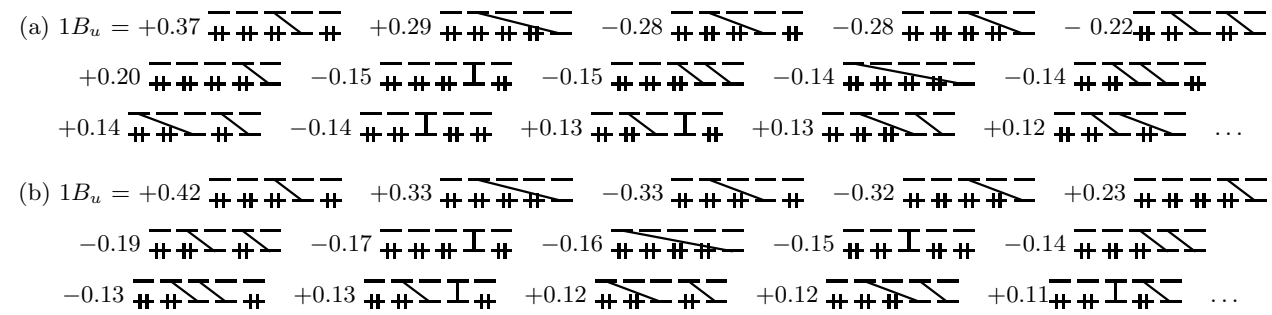

FIG. 6: The $1B_u$ wavefunctions for the N = 10 (a) polyene, and (b) substituted polyene within the minimal basis calculation, for $U = 6$ eV. Notice that the wavefunctions are similar in nature.

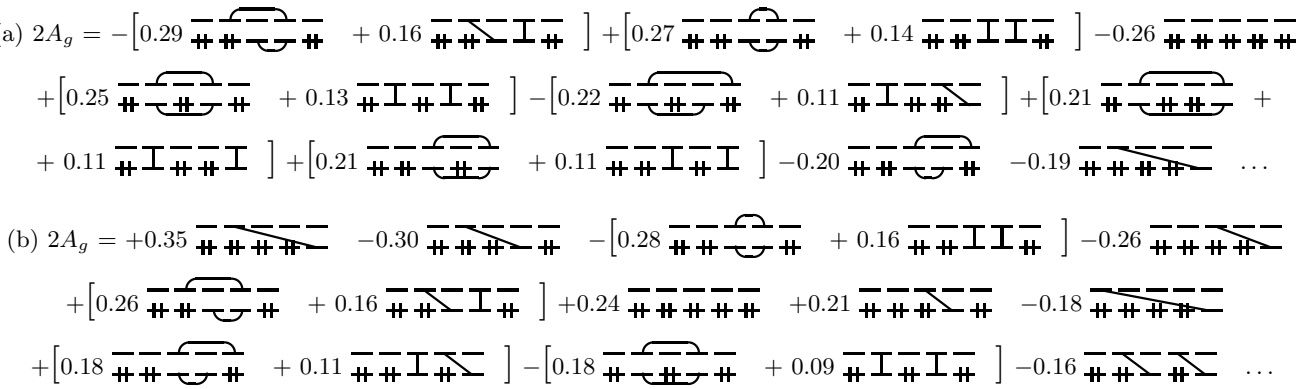

FIG. 7: The $2A_g$ wavefunctions for the N = 10 (a) polyene, and (b) substituted polyene within the minimal basis calculation, for $U = 6$ eV. Pairs of diagrams within the square parentheses occur as nearly 2:1 linear combinations, reflecting TT character. Note that the two wavefunctions are now very different, with CT contribution in (b) much larger than in (a).

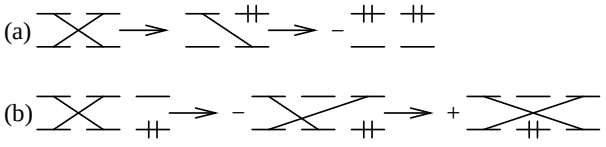

FIG. 8: CI channels that lower the energy of the $2A_g$. Arrows have the same meaning as in Fig. 3. (a) The CI process between the two-unit symmetric 2e–2h excitation and the quadruple excitation. (b) Similar CI process in the three-unit case that gives the symmetric 2e–2h diagram with long bonds.

to the Simpson ground state, their relative weights (more precisely, the relative weights of the TT diagrams with long bonds) in the exact $2A_g$ can be large (see Fig. 7). This is because of the degeneracy of all 2e–2h VB diagrams with crossed bonds within $H_{ee} + H_{1e}^{intra}$ which makes CI channels of the type in Fig. 8(b) extremely important. Second, the relative signs of the diagram with nearest neighbor crossed bonds and the diagram with long crossed bonds in Fig. 8 are the same. The same sign between them signifies constructive interference between the CI channels in Fig. 3(a) and Fig. 8(b), and as seen in Fig. 7, all TT diagrams have the same sign in the $2A_g$ wavefunction (TT $\otimes$ CT diagrams, defined in the above as TT-type diagrams that are accompanied by CT, as is true for the pair within the first parentheses in Fig. 7, can have opposite signs due to the additional CT), while the relative sign of the Simpson ground state is opposite (the relative sign of the Simpson ground state and the diagrams with crossed bonds are the same in the $1A_g$, as suggested by the CI channels; see reference 13).

In order to understand the role of additional MOs in polydiethylene-acetylene we will use the underlying information in Fig. 8. Two classes of 2e–2h excitations are relevant for the $2A_g$ – $1B_u$ crossover in the substituted polyene, intra- and interunit. The former are reached by application of H_{ee} (all terms in Eq. (1c)) to the Simpson ground state, the latter once again through two applications of H_{1e}^{inter}. The intramolecular 2e–2h excitations that are relevant for the $2A_g$ – $1B_u$ crossover are known from the existing literature on CI calculations using the MO basis for small molecules[25]. As far as the interunit high energy 2e–2h excitations are considered, the following is obvious from the previous sections and reference 13:

The only interunit 2e–2h VB diagrams that are relevant for the $2A_g$ – $1B_u$ crossover are the ones with

crossed bonds between units, since these are the only interunit diagrams that are charge-neutral. Strong CI involving diagrams with crossed bonds is essential for having contributions from higher energy TT diagrams.

Having identified the class of 2e–2h diagrams within the complete basis that may be relevant for the $2A_g$ – $1B_u$ crossover we note the following. Unless the higher energy 2e–2h diagrams are directly coupled to the lower energy 2e–2h diagrams by H_{ee} or H_{1e}^{inter} they have a very weak effect on $E(2A_g)$. In the absence of CI between the high and low energy diagrams, we have a nearly block-diagonal Hamiltonian, with each block containing its own set of excitations, with only the matrix elements of the Simpson ground state linking the blocks. Thus the $2A_g$ wavefunction continues to have strong CT contribution as shown in Fig. 6. Thus $E(2A_g)$ is lowered only if there exists CI channels analogous to those in Fig 8 that couple the high and low energy VB diagrams with crossed bonds. This leads to our second conclusion:

Unless the high energy relevant 2e–2h diagrams, containing intra- or interunit two-excitations, are coupled to the low energy diagrams with crossed bonds through two applications of H_{1e}^{inter}, they play an insignificant role in the $2A_g$ – $1B_u$ crossover.

We have limited ourselves only to second order processes between excitations (fourth order from the ground state) in the above, since if the higher energy diagrams are coupled in even higher order, their effects on $E(2A_g)$ are even weaker than quadruple excitations involving the minimal basis. Also, the couplings have to be necessarily through H_{1e}^{inter}, since all couplings through H_{ee} are intra-unit only. The above restrictions allow us to severely restrict our search for relevant high energy 2e–2h excitations and still reach the correct overall conclusion concerning the role of MOs beyond the minimal basis. In the following we discuss the case of the two-unit system first, followed by the more general case of arbitrary chain length. Our overall conclusion is that because of the *local* nature of H_{1e}^{inter} within the VB exciton basis, the effect of the couplings with the high energy 2e–2h diagrams in long chains is very weak. Because of the very detailed nature of the discussions that follow, we have given a summary of these discussions in the last subsection.

A. Two units: Coupling to intra-unit 2e–2h states

Exact $2A_g$ wavefunctions for small polyenes, obtained by FCI using the MO basis have been obtained by Schulten et. al.[25]. The dominant components of the $2A_g$ in molecular hexatriene are shown in Fig. 9(a) – (d). Of these, (a) is a superposition of 1e–1h excitations that can only *increase* $E(2A_g)$. As shown in Fig. 9(e) this 1e–1h configuration is coupled to intermolecular CT states in first order by H_{1e}^{inter}. The 2e–2h configuration (b) has been retained in our minimal basis calculation. This leaves the molecular configurations (c) and (d) in Fig. 9, and as shown in Fig. 9 (f) and (g), these are coupled

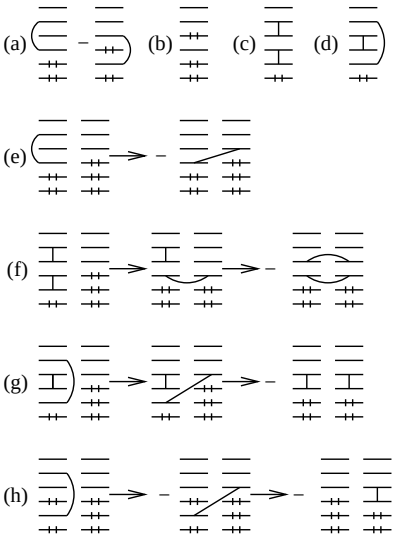

FIG. 9: (a) - (d): Intraunit excitations that dominate the molecular $2A_g$ in hexatriene. All 6 MOs are shown now. The lowest three in each unit are bonding MOs, while the upper three are antibonding MOs. (e): CI channel between one of the single excitations of (a) and a minimal basis CT diagram, for the two-unit system. (f) and (g): CI channels between intraunit 2e–2h excitations and the two components of the TT diagram within the minimal basis, also for the two-unit case. (h) CI channels between higher energy B_u Frenkel configuration and the minimal basis B_u Frenkel configuration. Arrows have the usual meaning in (e) – (h).

to components of the TT diagrams in the minimal basis by H_{1e}^{inter} in second order. Thus both 1e–1h and 2e–2h higher energy molecular A_g excitations are coupled to the minimal basis A_g diagrams, and without actual calculation, it is difficult to say which of the two CI processes involving the molecular A_g states shown in Fig. 9 will dominate near $U = U_c$. Furthermore, there occurs also CI between higher molecular B_u configurations and the minimal basis Frenkel configurations, as is shown in Fig. 9(h), and this process will lower $E(1B_u)$, which will have a larger bandwidth upon including all MOs. This last result was also pointed out in references 6,7 from transition dipole moment calculations.

The most important conclusion that one draws from Fig. 9 is that all interactions between minimal basis diagrams and the molecular diagrams are strictly local. The very nature of the CI process is such that the configurations that occur in the molecular $2A_g$ have matrix elements only with minimal basis TT diagrams in which the two triplet excitations occur on nearest neighbor units.

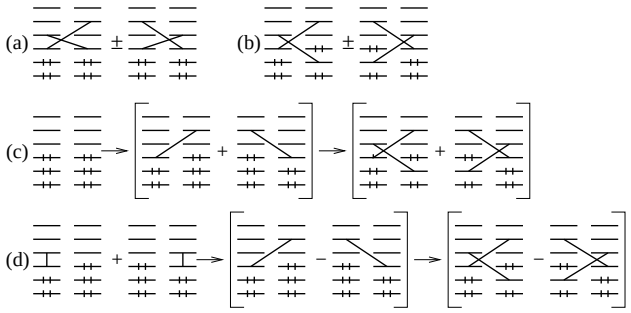

FIG. 10: (a) and (b): Superpositions of asymmetric 2e–2h exciton basis VB diagrams with crossed bonds, for the two-unit case. There are many such diagrams and their superpositions occur in both A_g and B_u subspaces, as is shown for one of the superpositions in (c) and (d) (see text).

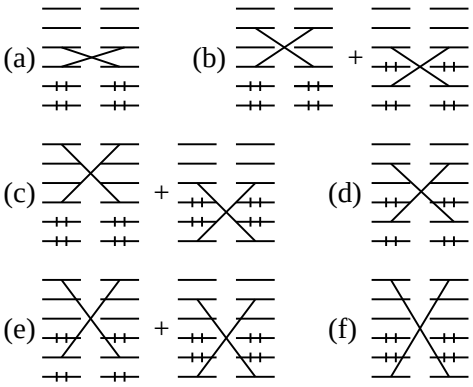

FIG. 11: Symmetric 2e–2h VB diagrams with crossed bonds in the two-unit oligomer of the substituted polyene. (a) is the minimal basis diagram. (b) – (f): high energy diagrams ignored in the minimal basis calculation.

B. Two units: Coupling to intermolecular 2e–2h states

Two-unit VB diagrams with crossed bonds can be classified as symmetric or asymmetric with respect to the mirror plane between the units. Both even and odd superpositions of the asymmetric VB diagrams are then possible, and these VB diagrams therefore occur in both A_g and B_u subspaces. Examples of such asymmetric VB diagrams involving MOs beyond the HOMO and LUMO are shown in Fig. 10(a) and (b). The simplest way to confirm that the superpositions shown do occur in both subspaces is to apply H_{1e}^{inter} twice on either the Simpson ground state (for occurrence in the A_g subspace) or the Frenkel exciton state (for occurrence in the B_u subspace). The application of H_{1e}^{inter} in this multi-MO case is achieved through Eqs. 7 and 9, and the signs originate from the different signs for each $\psi^{\dagger}_{1,k,\sigma}\psi_{2,k',\sigma}$ or $\psi^{\dagger}_{2,k,\sigma}\psi_{1,k',\sigma}$. This is done for the superposition of Fig. 10(a) in Fig. 10(c) and (d). The occurrence of the asymmetric VB diagrams in both A_g and B_u subspaces indicates that they play no significant role in the $2A_g$ – $1B_u$ crossover, and including them in our numerical calculations would not have altered the value of U_c in N = 4.

More important in the present context are therefore the symmetric TT diagrams. We have shown in Fig. 11 the corresponding diagrams with crossed bonds. These symmetric diagrams occur only in the A_g subspace and can in principle lower the energy of the $2A_g$. VB diagram 11(a) is the lowest energy diagram with crossed bonds, and we are interested in determining whether this diagram is coupled to any of the diagrams (b) – (f) in Fig. 11.

Three out of the five sets shown in Fig. 11, sets (d), (e) and (f), *cannot* have matrix elements of H_{1e}^{inter} with VB diagram (a) in second order, from orbital occupancies alone. This is because two applications of H_{1e}^{inter} can change the occupancies of only two MOs, while the VB diagrams in (d), (e) and (f) differ from diagram (a) by occupancies of four orbitals. This leaves only the diagrams in (b) and (c), which *are* coupled to the diagram in (a) once nonorthogonality of the VB basis functions is taken into consideration (see Fig. 3(e)), as is shown in the two CI channels in Fig. 12(a) and (b). The final VB diagram in Fig. 12 has nonzero overlap with diagram (a) in Fig. 11, and hence it might be thought that the CI processes shown can reduce $E(2A_g)$.

This is where the signs of the final diagrams in all CI channels become important. The minus sign in front of the final VB diagram in Fig. 12(a) and (b), taken together with the overlap of –1/2 between this diagram with noncrossing bonds and diagram 11(a), indicates that the diagram 11(a) is generated with a *plus* sign from these CI processes. This is in contrast to the CI process in Fig. 3(a) where diagram 11(a) is generated with a minus sign. There is thus destructive interference between the CI channels and the overall absolute "yield" of the low energy diagram with crossed bonds, starting from the Simpson ground state, *decreases* when CI channels involving the two higher energy symmetric diagrams (c) and (e) in Fig. 11 are included. Conversely, the relative weight of the Simpson ground state *decreases* in the $2A_g$, and $E(2A_g)$ *increases*. This interpretation of the CI process is unconventional but is perfectly valid (as can be readily ascertained by constructing and solving a Hamiltonian matrix that includes all the diagrams and CI channels shown in Figs 3 and 11, to determine the extent of mixing between the Simpson ground state and the low energy diagram with crossed bonds when the interfering channels of Fig. 12 are included) since the Hamiltonian matrix in the exciton VB basis is constructed essentially from the linear relationships shown in Figs. 3 and 12.

There is an alternate way to arrive at the same conclusion, which uses the relationship between VB diagrams in

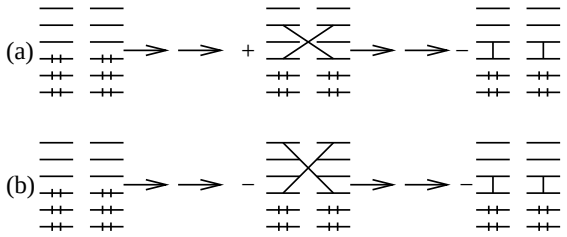

FIG. 12: CI processes involving two of the four symmetric VB diagrams of Fig. 11 that are coupled to the minimal basis symmetric 2e–2h diagram of Fig. 11(a) (see text). The double arrows denote two consecutive applications of H_{1e}^{inter}, promoting interunit CT in opposite directions. Plus and minus signs are consequences of applying Eq. 9. Similar CI processes involving the other two symmetric VB diagrams of Fig. 11 also give the same final diagram with minus sign.

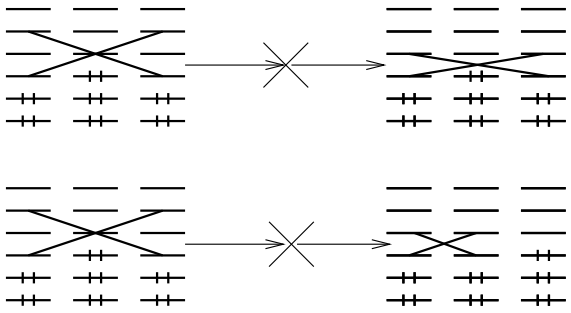

FIG. 13: The absence of coupling in second order between high energy long bonded 2e–2h VB diagram with crossed bonds and minimal basis VB diagrams with crossed bonds. Two applications of H_{1e}^{inter} on the diagram on the left does not generate either of the two diagrams on the right.

exciton basis and configuration space. We have already remarked that the singly excited units in the Frenkel exciton diagrams of Fig. 3 are ionic. In the case of polyenes, each singly excited unit is the superposition of ionic configurations 20 – 02, where the numbers denote atomic site occupancies. Thus two singly excited units contain (20 – 02)(20 – 02), i.e., the ionic configurations 2020, 2002, 0220 and 0202, and it is only the superposition in Fig. 3(d) that cancels these ionic contributions and gives the covalent VB diagram. Configuration mixing of the type in Fig. 12 therefore involves ionic diagrams at energy $2U$ (as opposed to covalent diagrams at zero energy), and hence can only increase $E(2A_g)$.

Our overall conclusion then is that already at the level of two units, we find that interunit high energy diagrams with crossed bonds play a weak role, and only couplings with intraunit excitations can perhaps lower $E(2A_g)$ [note that such couplings will also lower $E(1B_u)$, see Fig. 9(h)]. In such a short system, the role of intraunit 2e–2h excitations can be strong. If all MOs are included in a FCI calculation, it is possible that the true $2A_g$ is below the true $1B_u$ in N = 4, although the difference in their energies should be considerably smaller than in butadiene. Conversely though, if the molecular unit is such that the molecular $2A_g$ is *higher* in energy than the molecular $1B_u$, our discussion indicates that the $2A_g$ in the coupled system must necessarily be higher in energy than the corresponding $1B_u$. This is in agreement with our previous calculations on oligomers of PDPA[6,7] that used a multiple reference double-CI approach using a completely delocalized MO basis, and that found that the oligomer $2A_g$ is above the oligomer $1B_u$. The unit in PDPA is trans-stilbene, in which the molecular $2A_g$ is higher than the molecular $1B_u$.

C. Longer chains: Coupling to interunit 2e–2h states

For longer chains we focus on interunit 2e–2h VB diagrams only, since all interactions involving molecular 2e–2h states are restricted to minimal basis diagrams with nearest neighbor TT bonds. As discussed in the above, CI processes of the type shown in Fig. 8(b) are particularly important, because of the degeneracy between the short and long-bonded crossed diagrams. The nature of the exact $2A_g$ here and in reference 13 both indicate this. One can then visualize such CI processes involving all pairs of MOs k, k', which generate diagrams with long crossed bonds in longer chains, with the relative weights of the diagrams with short crossed bonds spanning two units gradually decreasing with chain length. Whether or not these diagrams with long crossed bonds are coupled to the minimal basis TT diagrams then decide how strongly the calculated minimal basis U_c is affected.

The classification of intermolecular 2e–2h VB diagrams as mirror plane symmetric or asymmetric persists in longer chains. Consider first the class of symmetric VB diagrams with long crossed bonds between distant units. Between any pair of molecular units there are as many of these as in Fig. 11. Since, however, H_{1e}^{inter} consists of nearest neighbor CT only, there are *no* symmetric diagrams with long bonds that are coupled to the lowest energy diagram with crossed bonds in second order now. This is shown in Fig. 13, where we have taken a three-unit version of one of the diagrams in Fig. 11 that did have coupling with the lowest energy diagram with crossed bonds. *Thus the minimal requirement of having the same occupancy in two out of four MOs is no longer sufficient to give coupling to the low energy diagram.*

New CI channels become important now with the asymmetric diagrams with crossed bonds. A subset of the asymmetric diagrams can now give long-bonded minimal basis TT diagrams, as shown in Figs 14(a) and (b), where we have given two such examples. *It should be*

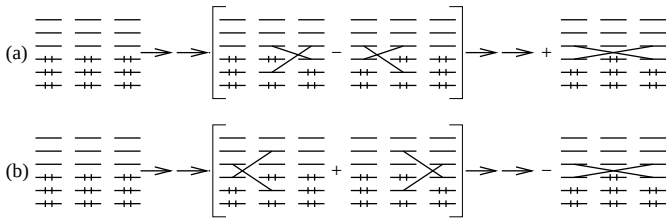

FIG. 14: Examples of CI processes that can generate the long bonded minimal basis VB diagram with crossed bonds, starting from the Simpson ground state, with high energy asymmetric 2e–2h diagrams with crossed bonds as the intermediate states. The double arrows again denote two consecutive applications of H_{1e}^{inter}. Note the opposite signs for the final product in the two channels, which is a consequence of charge-conjugation symmetry.

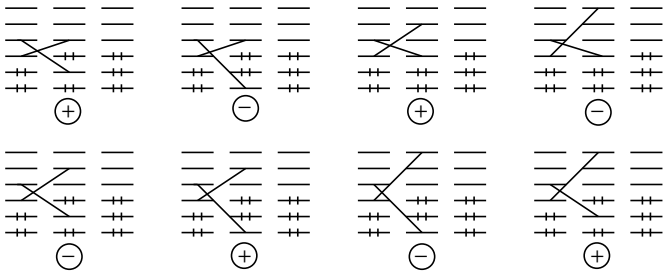

FIG. 15: Complete list of all asymmetric 2e–2h high energy VB diagrams with crossed bonds that are coupled to the Simpson ground state as well as the long bonded minimal basis VB diagram of Fig. 14, through CI processes of the type shown there. The plus or minus sign associated with each diagram corresponds to the sign on the minimal basis diagram, when the CI channels as in Fig. 14 are constructed, starting from the Simpson ground state in each case.

clear that the reverse of what is shown in this Figure, viz., generation of short-bonded minimal basis TT diagrams from long-bonded asymmetric diagrams is equally probable. In general high energy asymmetric diagrams with bonds spanning L units can give low energy symmetric diagrams with crossed bonds spanning L – 1 or L + 1 units. We discuss only the former, since the essential physics of all these processes are identical, and originate from charge-conjugation symmetry alone. Since we are interested in two consecutive CT processes in opposite directions only, the particular subset of asymmetric diagrams with short crossed bonds that can give the long bonded minimal basis TT diagram must satisfy a very strict condition, viz., *both the HOMO and the LUMO of one of the molecules in the initial state must be singly occupied.* For a reason that will be clear below, we have given in Fig. 14 the complete CT steps, starting from the Simpson ground state, that show how the asymmetric VB diagrams are generated in second order, and then another second order process gives the minimal basis VB diagram with long crossed bonds. The CI between the high energy asymmetric 2e-2h diagrams and the minimal basis diagram with crossed bonds clearly seems to suggest that the former are relevant, according to the two criteria of relevance we have proposed, and can lower E($2A_g$).

There are two reasons why CI processes such as those in Figs. 14 (and all similar processes in which asymmetric diagrams with crossed bonds of length L generate symmetric diagrams with minimal basis crossed bonds with lengths L+1 or L–1) contribute very weakly to the exact $2A_g$. First, the intermediate VB diagram with short crossed bonds in Fig. 8(b) is degenerate with the final TT state (as already pointed out in the above, this is what makes the contribution of long bonded TT diagrams in the $2A_g$ of polyenes large), while both the intermediate 2e–2h states in Fig. 14 have diagonal energies that are different from that of the final TT state. Even more importantly, we note that while the "yield" of the long bonded crossed diagram in Fig. 14(a) is positive, that in Fig. 14(b) is negative. *The opposite signs result from straightforward applications of Eq. (9) and are a consequence entirely of charge-conjugation symmetry, which determines the signs in these equations.* This has a very important implication for the extent of configuration mixing between the Simpson ground state and the long bonded TT diagram, viz., the configuration mixing induced by any one channel is reduced by the other. The simplest way to see this is to imagine that the two superpositions of asymmetric diagrams in Fig. 14(a) and (b) have the same diagonal matrix elements of $H_{ee} + H_{1e}^{intra}$. In that case, by operating with H_{1e}^{inter} we would have simply obtained the superposition of all four diagrams (the relative signs between which are determined entirely by Eq. (9)), and now a second application of H_{1e}^{inter} would simply give zero.

In Fig. 15 we have given all the asymmetric diagrams with crossed bonds in the three-unit chain that can be obtained by applying H_{1e}^{inter} twice to the Simpson ground state, and that in turn give the long-bonded minimal basis diagram with crossed bonds when further operated on by H_{1e}^{inter} (in each case we have given one diagram only, but superpositions of the type in Fig. 14 are being implied). The positive and negative sign associated with each diagram is the sign on the long bonded final diagram when CI channels as in Fig. 14 are constructed with these diagrams as intermediate states. Not surprisingly, the total number of such diagrams in Fig. 15 is even. Taken together with the fact that the configuration mixing between the Simpson ground state and the long-bonded TT diagram due to any one of these channels is small to begin with (due to the nondegeneracy between the intermediate asymmetric state and the final state), the even number of channels, with half of them giving positive matrix elements and the other half giving negative implies a nearly total cancellation effect. Since the above result is a consequence of charge-conjugation symmetry alone, it remains valid for all sets of asym-

metric diagrams with crossed bonds, independent of the bond lengths. We therefore conclude that *exactly as the symmetric diagrams with long crossed bonds, the asymmetric diagrams with crossed bonds have very weak CI with the minimal basis TT diagrams in long chains.*

D. Summary

Our basic conclusion is that high energy intraunit 2e–2h excitations that have been ignored in our minimal basis calculations can affect the final results. However, couplings between these and minimal basis TT diagrams are strictly local, and moreover, due to the nondegeneracy between the molecular 2e–2h states and the minimal basis 2e–2h states the effect of this coupling on long chains should be weak. Recall, for example, that the relative weights of minimal basis TT diagrams with nonnearest neighbor bonds can continue to be relatively large even as the lengths of the interunit bonds keep increasing (see Fig. 7 and also reference 13), but the couplings in Fig. 9 are only to TT diagrams with nearest neighbor bonds. In contrast to the intraunit 2e–2h states, the coupling of the minimal basis TT diagrams to the interunit high energy 2e–2h VB diagrams is extremely weak. Indeed this latter coupling can even raise $E(2A_g)$ slightly in the case of two units. The weak coupling with high energy interunit states is a symmetry effect that will persist in any system which has spatial and charge-conjugation symmetries.

VI. CONCLUSION

In conclusion, we have analyzed the excited state ordering in finite chain analogs of the simplest model conjugated polymer with transverse π-conjugation within the dimerized Hubbard Hamiltonian. The system considered consists of a backbone polyene chain with ethylenic sidegroups. We developed a multilevel exciton basis description for the system, and within a minimal basis, which consists of the HOMO and the LUMO of each unit, we showed that the effective electron correlations in this substituted polyene is smaller than that in the unsubstituted polyene. The reason for this is that each carbon atom of the polyene is now replaced with multiple atoms over which a double occupancy is delocalized, thereby giving it a transverse bandwidth that lowers its energy[6]. Smaller effective correlations, in turn, suggests that the $2A_g$ is above the $1B_u$ in this class of materials, and that this provides an interesting route to obtain organic polymers that emit in the IR.

The chief advantage of the exciton basis approach is that the role of the high energy configurations that are ignored within the minimal basis calculations can be determined precisely, because of the local character of the basis functions, as well as the local nature of the configuration interaction within the Hubbard Hamiltonian. Our very detailed analysis here indicates that few of the high energy TT configurations that we ignore have CI in second order with the minimal basis TT configurations. In particular, the CI between interunit high and low energy TT diagrams is very weak. The only relevant CI between high and low energy states that can at all lower the energy of the polymer $2A_g$ involves the intraunit configurations that describe the molecular $2A_g$ state. Note that this already ensures the following result, viz., if the molecular unit is such that the molecular $2A_g$ is higher than the molecular $1B_u$, then since within the minimal basis the $2A_g$ is also higher than the $1B_u$, the overall $E(2A_g)$ is also higher than the overall $1B_u$. This in turn predicts that that $E(2A_g)$ must necessarily be larger than $E(1B_u)$ in PDPA, since the molecular $2A_g$ is higher than the molecular $1B_u$ in the fundamental unit trans-stilbene. Our conclusion here is in agreement with the previous conclusion about PDPA, which was arrived from computations only[6,7].

The molecular $2A_g$ configurations interact only with the minimal basis TT diagrams in which the two triplets occupy nearest neighbor units. In a long chain system, the relative weight of such TT diagrams with nearest neighbor bonds is small, since there exist in long chains TT diagrams with all possible bond lengths, and their contributions are comparable. At the same time, in the isolated real hexatriene molecule, which forms the unit in our model system, the lowest one- and two-photon states occur at a very high energy of ~ 5 eV, whereas the polymeric $1B_u$ and $2A_g$ occur below 1.6 eV, which is $E(1B_u)$ for t-PA. Thus any interaction between molecular and polymer states decreases progressively with increasing chain length, and we expect that even for our model system the minimal basis results are qualitatively correct. Importantly, of course, our model calculations are for the illustration of the principle only, and real systems in which the molecular $2A_g$ is higher than the molecular $1B_u$ can always be developed with suitable modification of the molecular unit. The real experimental challenge here is to develop systems in which steric interactions are small enough that oligomers with long conjugation lengths and small optical gaps can be synthesized. Finally, we mention that we have not discussed here known π-conjugated polymers with low band gaps, such as poly(isothianaphthene)[36] and poly(isonaphthothiophene)[37]. It is of interest that in these systems too there occur transverse conjugation over a few bonds in addition to the conjugation along the polymer axis, although the nature of the transverse conjugation is slightly different from that in our model system consisting of a substituted polyene. The electronic structures and the small optical gaps in these systems have been discussed within one-electron theory[38] and future theoretical work within many-electron approaches is clearly of interest.

VII. ACKNOWLEDGMENTS

Work in Arizona was supported by NSF DMR-0101659, NSF ECS-0108696 and by the ONR. Sandia is a multiprogram laboratory operated by Sandia Corporation, a Lockheed Martin Company, for the United States Department of Energy under Contract DE-AC04-94AL85000.

[1] R. H. Friend et al., Nature **397**, 121 (1999).
[2] N. Tessler, G. J. Denton, and R. H. Friend, Nature **382**, 121 (1996).
[3] F. Hide et al., Science **273**, 1833 (1996).
[4] S. Frolov et al., Phys. Rev. Lett. **78**, 729 (1997).
[5] F. Capasso, C. Gmachl, D. L. Sivco, and A. Y. Cho, Physics Today **55**, 34 (2002).
[6] A. Shukla and S. Mazumdar, Phys. Rev. Lett. **83**, 3944 (1999).
[7] H. Ghosh, A. Shukla, and S. Mazumdar, Phys. Rev. **B 62**, 12763 (2000).
[8] K. Tada et al., Proc. SPIE-Int. Soc. Opt. Eng. **3145**, 171 (1997).
[9] I. Gontia et al., Phys. Rev. Lett. **82**, 4058 (1999).
[10] R. Hidayat et al., Phys. Rev. **B 61**, 10167 (2000).
[11] Z. G. Soos, S. Etemad, D. S. Galvao, and S. Ramasesha, Chem. Phys. Lett. **194**, 341 (1992).
[12] Z. G. Soos, S. Ramasesha, and D. S. Galvao, Phys. Rev. Lett. **71**, 1609 (1993).
[13] M. Chandross, Y. Shimoi, and S. Mazumdar, Phys. Rev. **B 59**, 4822 (1999).
[14] W. T. Simpson, J. Am. Chem. Soc. **73**, 5363 (1951).
[15] I. Ohmine, M. Karplus, and K. Schulten, J. Chem. Phys. **68**, 2298 (1978).
[16] K. Ishida, H. Aoki, and T. Ogawa, Phys. Rev. **B 52**, 8980 (1995).
[17] F. B. Gallagher and F. C. Spano, Phys. Rev. **B 53**, 3790 (1996).
[18] D. Mukhopadhay, G. W. Hayden, and Z. G. Soos, Phys. Rev. **B 51**, 9476 (1995).
[19] W. Barford and R. Bursill, Chem. Phys. Lett. **268**, 535 (1997).
[20] M. Y. Lavrentiev, W. Barford, S. J. Martin, H. Daly, and R. J. Bursill, Phys. Rev. **B 59**, 9987 (1999).
[21] M. A. Martin-Delgado, G. Sierra, S. Pleutin, and E. Jeckelmann, Phys. Rev. **B 61**, 1841 (2000).
[22] M. J. Rice and Y. N. Gartstein, Phys. Rev. Lett. **73**, 2504 (1994).
[23] A. Chakrabarti and S. Mazumdar, Phys. Rev. **B 59**, 4839 (1999).
[24] J. Knoester and F. Spano, Physical Review Letters **74**, 2780 (1995).
[25] B. S. Hudson, B. E. Kohler, and K. Schulten, Excited States **5**, 1 (1982).
[26] B. Lawrence et al., Phys. Rev. Lett. **73**, 597 (1994).
[27] Z. G. Soos and S. Ramasesha, Phys. Rev. **B 29**, 5410 (1984).
[28] Z. Shuai, J. L. Bredas, S. K. Pati, and S. Ramasesha, **56**, 9298 (1997).
[29] M. Y. Lavrentiev and W. Barford, Phys. Rev. **bf B 59**, 15048 (1999).
[30] T. Ishiguro, K. Yamaji, and G. Saito, in *Organic Superconductors, Second Edition* (Springer-Verlag, Berlin, 1998).
[31] S. Ramasesha and B. Srinivasan, Solid St. Commun. **81**, 831 (1992).
[32] R. Pariser and R. G. Parr, J. Chem. Phys. **21**, 466 (1953).
[33] J. A. Pople, Trans. Farad. Soc. **49**, 1375 (1953).
[34] P. Tavan and K. Schulten, Phys. Rev. **B 36**, 4337 (1987).
[35] F. Guo, M. Chandross, and S. Mazumdar, Phys. Rev. Lett. **74**, 2086 (1995).
[36] M. Kobayashi, N. Colaneri, M. Boysel, and A. J. Heeger, J. Chem. Phys. **82**, 5717 (1985).
[37] Y. Ikenoue, Synth. Metals **35**, 263 (1990).
[38] Y. Lee, M. Kertesz, and R. Elsenbaumer, Chem. Mater. **2**, 526 (1990).